Supplementary Information

Quantifying the Reaction Mechanisms of a High-Capacity CuP_2/C Composite Anode for Potassium Ion Batteries

Chen Zhao,[a,b,c] Huixin Chen,[b,c] Haodong Liu,[d] Liang Yin,[f] Qiaobao Zhang,[g] Sicen Yu,[d] Ping Liu,[d] Guiming Zhong,[*,a,b,c,h] Can-Zhong Lu,[*,a,b,c,h] Yong Yang[e]

[a] College of Chemistry, Fuzhou University, Fuzhou 350108, Fujian, China

[b] CAS key Laboratory of Design and Assembly of Functional Nanostructures, and Fujian Provincial Key Laboratory of Nanomaterials, Fujian Institute of Research on the Structure of Matter, Chinese Academy of Sciences, Fuzhou 350002, Fujian, China

[c] Xiamen Key Laboratory of Rare Earth Photoelectric Functional Materials, Xiamen Institute of Rare Earth Materials, Haixi institutes, Chinese Academy of Sciences, Xiamen 361021, Fujian, China

[d] Department of Nanoengineering, University of California San Diego, La Jolla, CA 92093, United States

[e] State Key Lab of Physical Chemistry of Solid Surfaces, Collaborative Innovation Center of Chemistry for Energy Materials and Department of Chemistry, Xiamen University, Xiamen 361005, Fujian, China

[f] X-ray Science Division, Advanced Photon Source, Argonne National Laboratory, Lemont, Illinois 60439, United States

[g] Department of Materials Science and Engineering, College of Materials, Xiamen University, Xiamen 361005, Fujian, China

[h] University of Chinese Academy of Sciences, Beijing, 100049, China

This file includes:

1. Experimental section.
2. Figure S1. The characterization of as-prepared of CuP_2 and CuP_2/C materials: Raman spectra, XPS Cu 2*p*, XPS C 1*s* and XPS O 1*s* spectra.
3. Figure S2. Structural representation of CuP_2.
4. Figure S3. Laboratory XRD patterns of CuP_2/C electrodes at selected states during first cycle and second discharge.
5. Figure S4. Synchrotron XRD patterns of CuP_2/C electrodes at 1D0V state; Standard PDF cards of KPO_2F_2, K_2PO_3F and $K_2P_2O_5F_2$.
6. Figure S5. XRD patterns of the prepared K-P alloys and ^{31}P NMR spectra.
7. Figure S6. Comparison of fitting results by using 3 peaks and 4 peaks at around 0 ppm at 1C1.2V state.
8. Figure S7. The structural evolution of CuP_2/C composite in the second discharge process by solid-state ^{31}P NMR spectroscopy.
9. Table S1. The element (C and O) analysis results of CuP_2 and CuP_2/C materials.
10. Table S2. The particle size distribution results of CuP_2 and CuP_2/C materials.
11. Table S3. The theoretical specific capacities of K-P alloys, such as KP, K_4P_3 and K_3P.
12. Table S4. The theoretical specific capacities of different components in the CuP_2/C composite.
13. Table S5. The quantitative fitting results of the spectra in Figure 4 (1^{st} cycle) and Figure S7 (2^{nd} discharge).
14. Fitting details.
15. Fitting figures.
16. References.

Experimental section

Materials synthesis. CuP_2 was synthesized by high-energy ball-milling. First, stoichiometric amounts of nano-copper (~ 500 nm, 99.9 %, Aladdin, China) and red phosphorus powders (98.9 %, Alfa Aesar, China) were mixed and put into a stainless-steel jar with a ball-to-powder mass ratio of 30:1. After sealing the jar in an argon-filled glovebox with oxygen and water levels all below 0.5 ppm, the ball-milling process was performed on a high-energy ball-milling (MITR-YXQM, China) for 24 h at 600 rpm to obtain CuP_2 material. CuP_2/C composite was prepared using the similar method. Briefly, CuP_2 (70 wt.%), Super P (15 wt.%) and reduced graphene oxide (15 wt.%, prepared by Hummer's method) were mixed and ball-milled under argon atmosphere to obtain the composite material.

Electrochemical measurements. The electrochemical performance of CuP_2/C material as an anode for PIBs was tested at 30 ^oC using 2025-type coin cells. The CuP_2/C electrodes were prepared by coating the slurry of 70 wt.% CuP_2/C composite, 15 wt.% carbon nanotubes and 15 wt.% cross-linked polymer binder of carboxymethylcellulose-citric acid (CMC-CA, 9:1, weight ratio) onto the Al disks, which were dried at 80 ^oC under vacuum overnight and then at 150 ^oC for 4 h to form 3D cross-linking networks. [1] All the cells were assembled in an argon-filled glove box, using 0.8 M KPF_6 in a mixed solvent of ethylene carbonate (EC) and diethyl carbonate (DEC) (1:1, in volume) as the electrolyte, potassium metal as the counter electrode, and glass fiber as the separator. The cells were (dis)charged galvanostatically in a voltage window of 0 to 3 V on a battery testing system (Shenzhen Neware, China). Specific capacity values were measured based on the total mass of the CuP_2/C composite. Cyclic voltammetry (CV) was carried out at a scan rate of 0.03 mV s^{-1} on a CHI 760E electrochemical workstation (Shanghai Chenhua, China).

Materials characterizations. The powder X-ray diffraction (XRD) patterns were collected from the Rigaku Miniflex 600 by using a Cu Kα radiation at 40

kV and 15 mA (λ_1= 1.540598 Å). Raman spectroscopies of as-prepared powder samples were taken on a BWS465-785S Raman system with an excitation at 725 nm laser radiation in a range of 200 to 2000 cm^{-1}. X-ray photoelectron spectroscopies (XPS) were performed on the ESCALAB 250Xi. The morphologies of prepared materials were studied by scanning electron microscopy (SEM, HITACHI S4800) and transmission electron microscopy (TEM, Talos-F200X). The diameter distribution of the materials was investigated by Brookhaven Omni after 30-minute sonication. For *ex-situ* studies, the cells were firstly cycled to certain (dis)charged states at 12.5 mA g^{-1} then disassembled inside the glovebox. And the electrodes were rinsed by dimethyl carbonate (DMC) then dried. The electrodes were sealed by Kapton films inside the glovebox for synchrotron XRD measurement. High-resolution synchrotron XRD patterns were collected at the 11-BM at the Advanced Photo Source of Argonne National Laboratory (λ_2= 0.457926 Å). The electrodes materials were scraped and filled into 1.3 mm rotors for solid-state NMR measurement. All the solid-state NMR experiments were performed on a Bruker 400 MHz AVANCE III spectrometer at a Larmor frequency of 162 MHz for ^{31}P. The ^{31}P magic angle spinning (MAS) NMR spectra were acquired using Hahn-echo pulse (90° pulse-τ-180° pulse-τ) under the spinning frequency of 55 kHz. π/2 pulse length of 1.6 us and recycle delay of 30-60 s were applied for complete relaxation of excited magnetization. The chemical shifts of ^{31}P were referenced to adenosine diphosphate (1 ppm). Additionally, standard K-P alloys were successfully produced with a stoichiometric amount of K metal and red P powders in a closed circumstance, then placed in a cube furnace filled with inert gas at high temperature, which were further characterized by XRD (polyurethane and Mylar films for protection) and solid-state NMR.

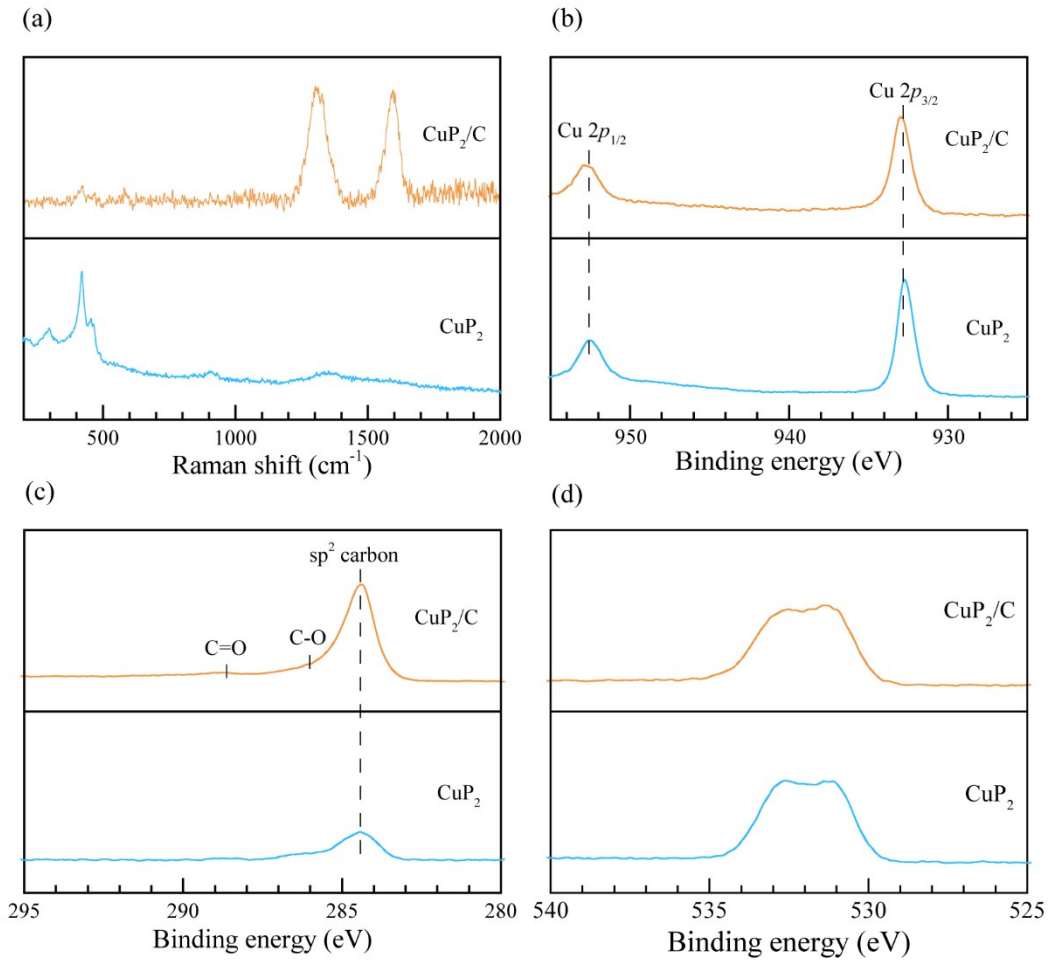

Figure S1. The characterization of as-prepared of CuP_2 and CuP_2/C materials: (a) Raman spectra, (b) XPS Cu 2*p*, (c) XPS C 1*s* and (d) XPS O 1*s* spectra.

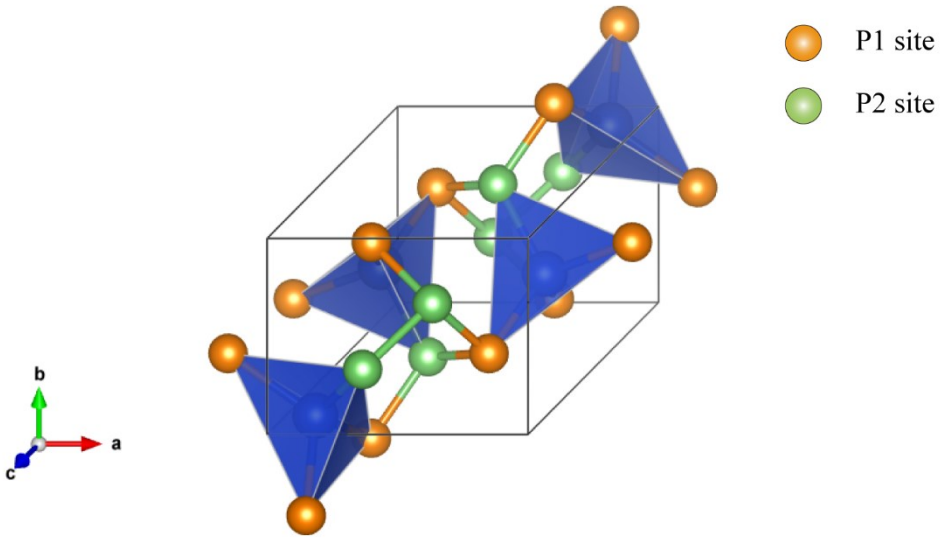

Figure S2. Structural representation of CuP_2 (P1 site: orange; P2 site: green).

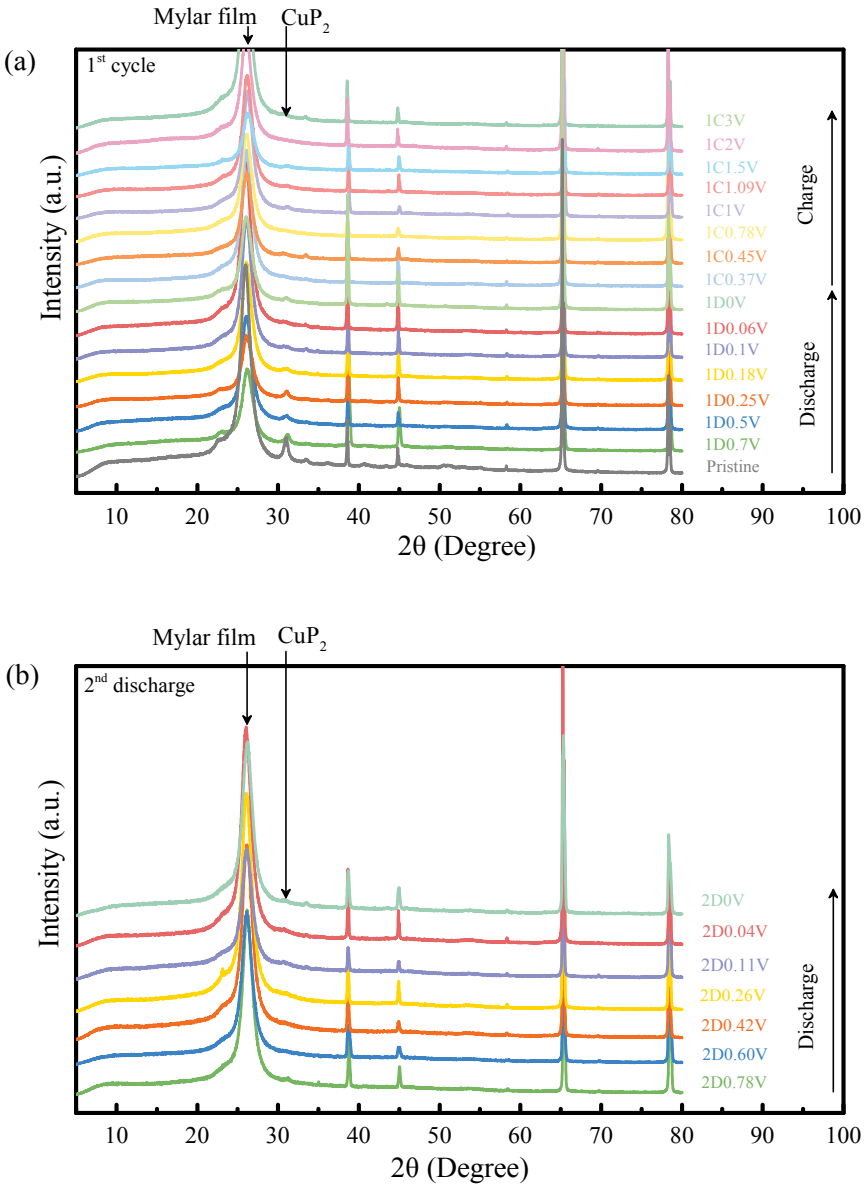

Figure S3. Laboratory XRD patterns of CuP_2/C electrodes at selected states during (a) first cycle and (b) second discharge.

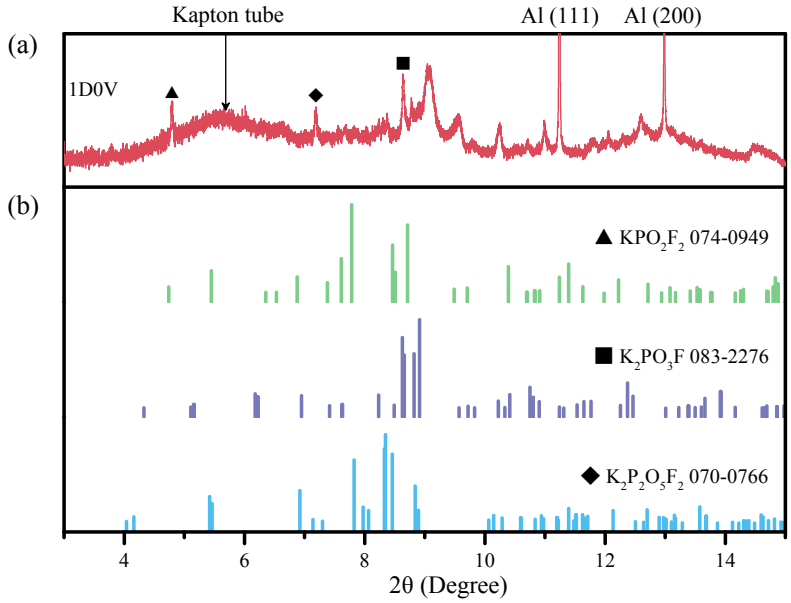

Figure S4. (a) Synchrotron XRD patterns of CuP_2/C electrodes at 1D0V state; (b) Standard PDF cards of KPO_2F_2, K_2PO_3F and $K_2P_2O_5F_2$.

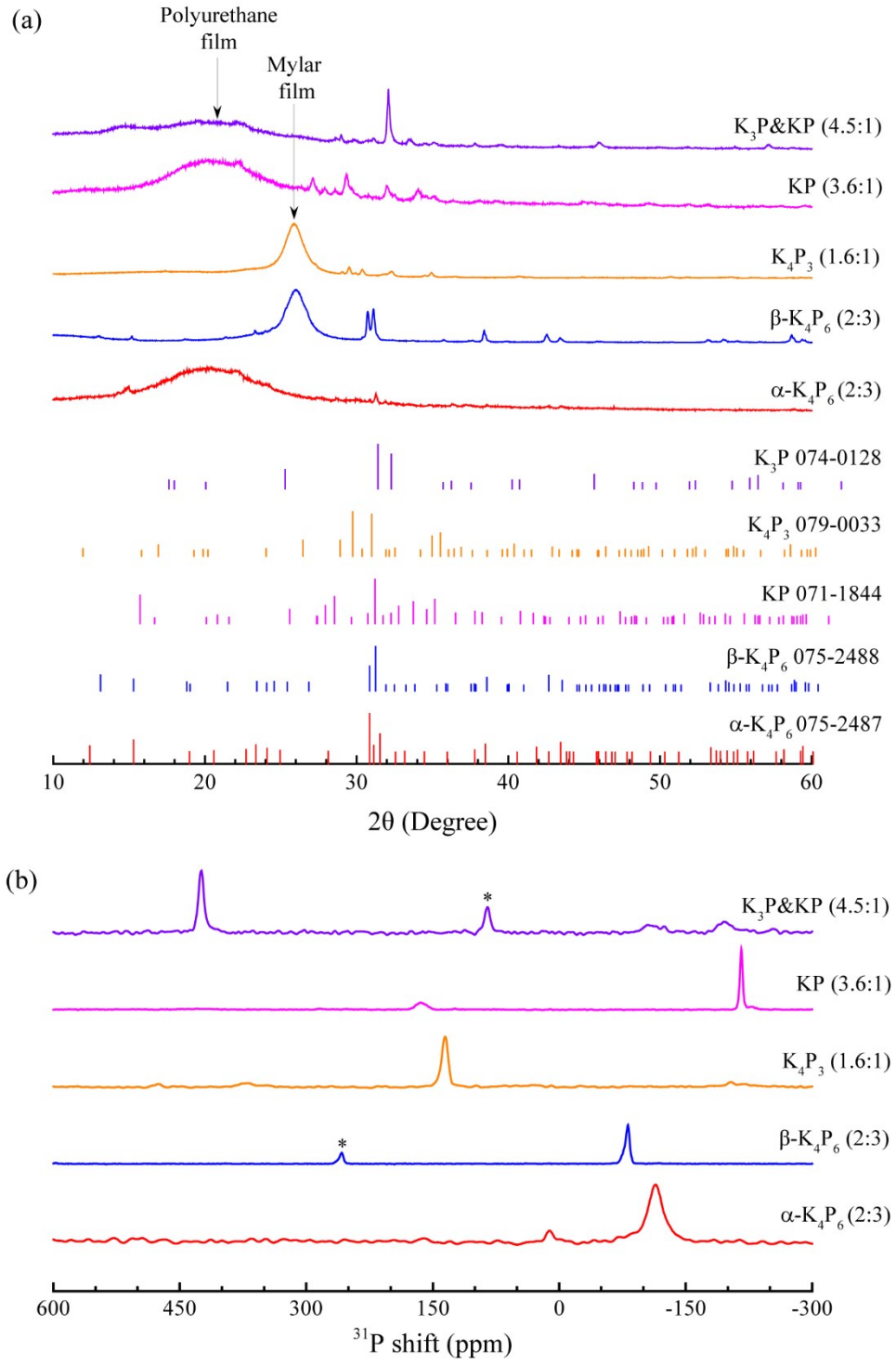

Figure S5. (a) XRD patterns of the prepared K-P alloys and the corresponding standard PDF cards; (b) ^{31}P NMR spectra. The asterisks indicate the spinning sidebands.

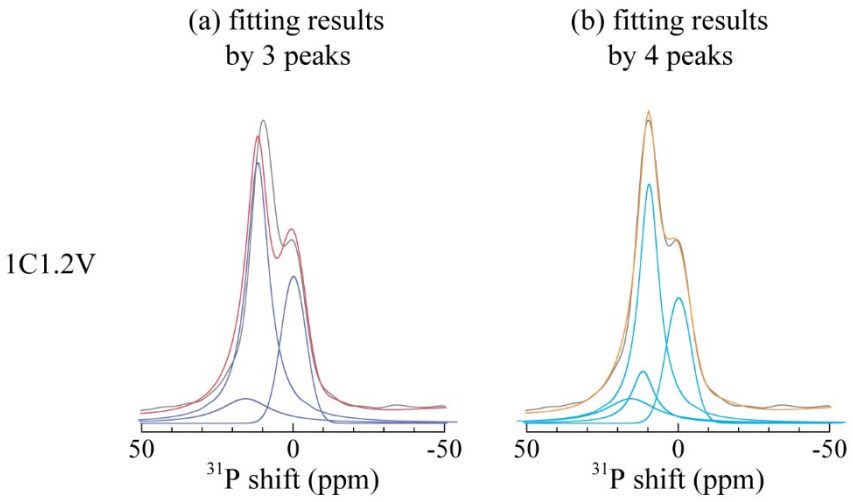

Figure S6. Comparison of fitting results by using (a) 3 peaks and (b) 4 peaks at around 0 ppm at 1C1.2V state.

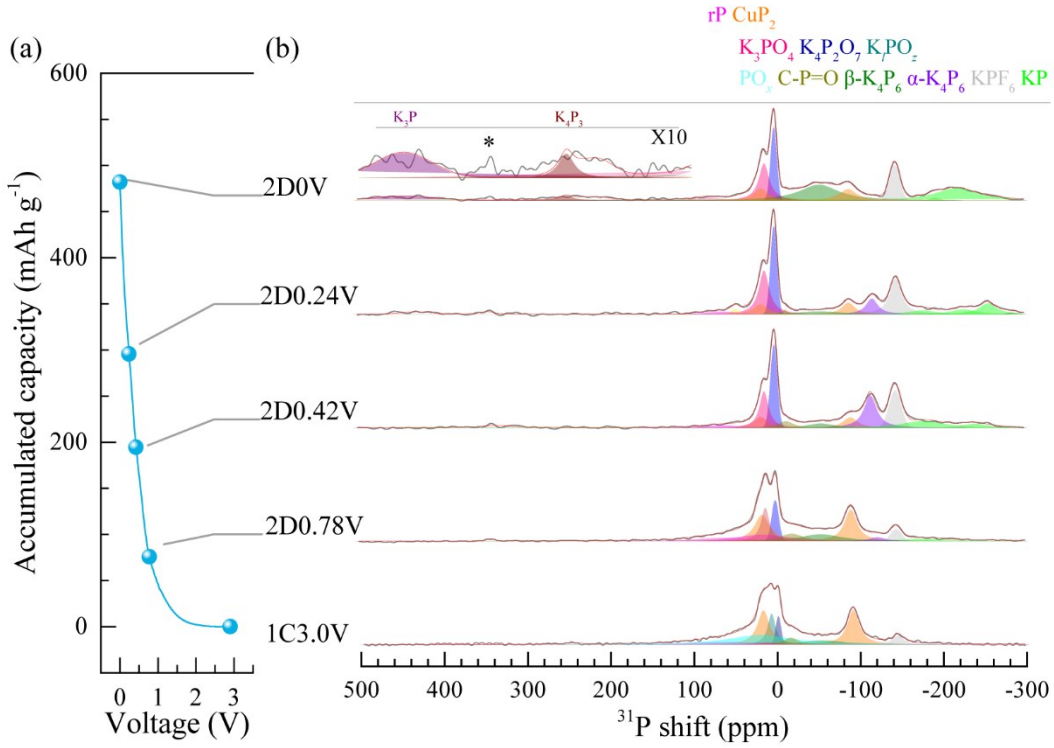

Figure S7. Tracking the structural evolution of CuP_2/C composite in the second discharge process by solid-state ^{31}P NMR spectroscopy: (a) The electrochemical profiles of the CuP_2/C electrode at a current of 12.5 mA g^{-1}; (b) Solid-state ^{31}P NMR spectra of the CuP_2/C electrodes at selected states (light grey colored peak at ~ -145 ppm: the residual KPF_6 originated from the electrolytes; purple colored area: K_3P; wine colored area: K_4P_3; magenta colored area: rP; orange colored area: CuP_2; pink colored area: K_3PO_4; navy colored area: $K_4P_2O_7$; dark cyan colored area: K_IPO_z; dark yellow colored area: C-P=O; cyan colored area: PO_x; olive colored area: a-K_4P_6; violet colored area: α-K_4P_6; green colored area: KP. The asterisks indicate the spinning sidebands).

Table S1. The elemental (C and O) analysis results of CuP_2 and CuP_2/C materials.

	CuP_2	CuP_2/C
C (%)	0.9	26.8
O (%)	2.2	7.4

Table S2. The particle size distribution results of CuP_2 and CuP_2/C materials.

	CuP_2	CuP_2/C
D_{10} (nm)	331.37	171.72
D_{50} (nm)	647.08	303.45
D_{90} (nm)	1264.34	536.22

Table S3. Calculated theoretical specific capacities of CuP_2 according to different products: KP, K_4P_3 and K_3P.

Compounds	KP	K_4P_3	K_3P
Capacity (mAh g^{-1})	427	569	1281

Table S4. The theoretical specific capacities of components in the CuP_2/C composite. Here, we take KP or K_4P_3 as the final product of phosphorus-based materials.

Compounds	CuP_2	rP	$PO_{3.4}$	C
Final products	KP	KP	KP, K_3PO_4, $K_4P_2O_7$	KC_8
Specific capacity (mAh g^{-1})	427	865	755	279
Mass percent in the composite	50.2%	3.5%	19.5%	26.8%
Capacity contributions (mAh g^{-1})	214.5	30.7	147.5	74.8

Compounds	CuP_2	rP	$PO_{3.4}$	C
Final products	K_4P_3	K_4P_3	KP, K_3PO_4, $K_4P_2O_7$	KC_8
Specific capacity (mAh g^{-1})	569	1153	755	279
Mass percent in the composite	50.2%	3.5%	19.5%	26.8%
Capacity contributions (mAh g^{-1})	285.8	40.9	147.5	74.8

The NMR fitting result of CuP_2/C material has shown that the atomic ratio of P in CuP_2, rP (red P) and PO_x are 7:1:2. In combination with the elemental analysis results (Table S1) that show that the content of oxygen and carbon is 27.8% and 7.4%, respectively, we can calculate that the *x* value in PO_x is ~ 3.4, and conclude that the contents of CuP_2, rP, $PO_{3.4}$ and C in the composite are 50.2%, 3.5%, 19.5% and 26.8%, respectively.

Besides, the NMR fitting results of potassiated electrodes have indicated that the atomic ratio of P in K_3PO_4 and $K_4P_2O_7$ is about 1.3:1. Then we obtain the reaction equation of $PO_{3.4}$ (Equation (1)) and calculate the specific capacity of $PO_{3.4}$ to be 755.1 mAh g^{-1} assuming the final products are KP, K_3PO_4 and $K_4P_2O_7$, which is higher than that of CuP_2 (427 mAh g^{-1}, taking KP as the final product). The theoretical capacity contribution of $PO_{3.4}$ in the composite is 147.5

mAh g^{-1} (Table S5).

$$5.12\ PO_{3.4} + 12.32\ K \rightleftharpoons 2.6\ K_3PO_4 + K_4P_2O_7 + 0.52\ KP \quad (1)$$

Table S5. The quantitative fitting results of solid-state ^{31}P NMR spectra.

	CuP_2	rP	K_lPO_z	PO_x	K-O-P	α-K_4P_6	a-K_4P_6	KP	K_4P_3	K_3P
OCV	69.07	13.01	0	17.92	0	0	0	0	0	0
1D0.5V	63.48	8.53	0	3.54	20.19	0	3.54	0.73	0	0
1D0.33V	65.47	6.97	0	4.22	20.8	0	1.37	1.16	0	0
1D0.18V	55.98	6.56	0	1.59	26.35	1.27	2.43	5.82	0	0
1D0.1V	44.24	4.16	0	0.85	26.76	1.6	10.98	11.41	0	0
1D0.05V	32.24	0	0	2.85	25.18	0	27.08	9.38	0	3.27
1D0V	22.4	0	0	2.1	22.61	0	27.13	19.24	1.16	5.36
1C0.54V	17.23	0	0	2.7	30.29	3.38	12.27	28.04	1.01	5.07
1C0.78V	19.88	0	0	5.77	32.27	4.29	6.99	30.8	0	0
1C0.96V	21.69	4.91	0	1.6	30.14	6.51	9.13	26.03	0	0
1C1.2V	20.39	3.13	26.3	2.43	23.64	1.16	9.85	13.09	0	0
1C3.0V	36	5.36	10.94	33.15	6.56	0	7.99	0	0	0
2D0.78V	34.13	7.37	0	19.5	19.5	2.59	11.51	5.39	0	0
2D0.42V	15.93	4.8	0	5.04	31.73	18.62	5.62	18.27	0	0
2D0.24V	18.15	4.5	0	1.72	37.88	9.67	6.75	21.32	0	0
2D0V	13.95	0	0	1.14	24.28	0	20.25	29.24	7.85	6.1

Fitting details

In the text, Figure 4 and S7 display the mass-normalized solid-state ^{31}P NMR spectra of the electrodes and the corresponding deconvolution plots for the first cycle and the second discharge process of CuP_2/C. The spectra exhibit a very broad shift range from 500 to -300 ppm and include several peaks. Therefore, a reasonable fitting strategy is very important to guarantee rational deconvolution results. The ^{31}P NMR spectrum of the pristine material in Figure 1c has shown that the ^{31}P resonances of CuP_2 are ~ 15.6 and ~ - 90.9 ppm with half-widths of ~ 20 ppm and integral ratio of 1:1. It also has shown a broad peak at around 10 ppm attributed to PO_x, and the resonances of red P are at 62.7 and -95.2 ppm. [2] The ^{31}P signal of residual KPF_6 from electrolyte is ~ -145 ppm. Then, we can well fit the spectrum of 1D0V by using these resonances with additional two peaks at ~ 11.6 and 0.7 ppm, a broad peak at -55 ppm, and several peaks from -180 to -275 ppm. The fitted peaks at ~ 11.6 and 0.7 ppm are highly consistent with the resonances of K_3PO_4 and $K_4P_2O_7$. [3-4] Of note, previous works have shown that the chemical shift may change for the counterpart nano or amorphous phase, and the half-width would largely broaden compared to that of counterpart crystalline compound due to the change of the local environment and increasing anisotropy. [5-6] Hence, we consider that the broad peak at ~ -55 ppm is probably due to the a-K_4P_6 (amorphous β-K_4P_6, similarly hereinafter). The signals covering from -180 to -275 ppm clearly show two sharp peaks at ~ -255 and -272 ppm, and two broad peaks at ~ -180 and -225 ppm for a well-converged fitting, which are attributed to the formation of KP. The different chemical shift and the broad line-width compared to the reference KP (-220 ppm) are likely due to the nonstoichiometric or amorphous properties of the KP phases. Noticeably, the peaks at ~ -255 and ~ -272 ppm show narrow line, inferring that the corresponding KP phases possess a relatively ordered structure, which is possibly crystalline. And the broad peaks at ~ -185 and -225 ppm are either

nano or amorphous KP phase. Another two peaks at ~ 210 and ~ 450 ppm are clearly observed, presenting relatively broad half-width. According to the reference spectra of crystalline K_4P_3 and K_3P that exhibit sharp peaks at 150 and 425 ppm, the broad signals at ~ 210 and ~ 450 ppm belong to the K_4P_3 and K_3P phases. As a result, by employing these settings, all the ^{31}P NMR spectra can be well-fitted, and providing an insightful quantitative analysis, which are shown in Figure 5.

Fitting figures

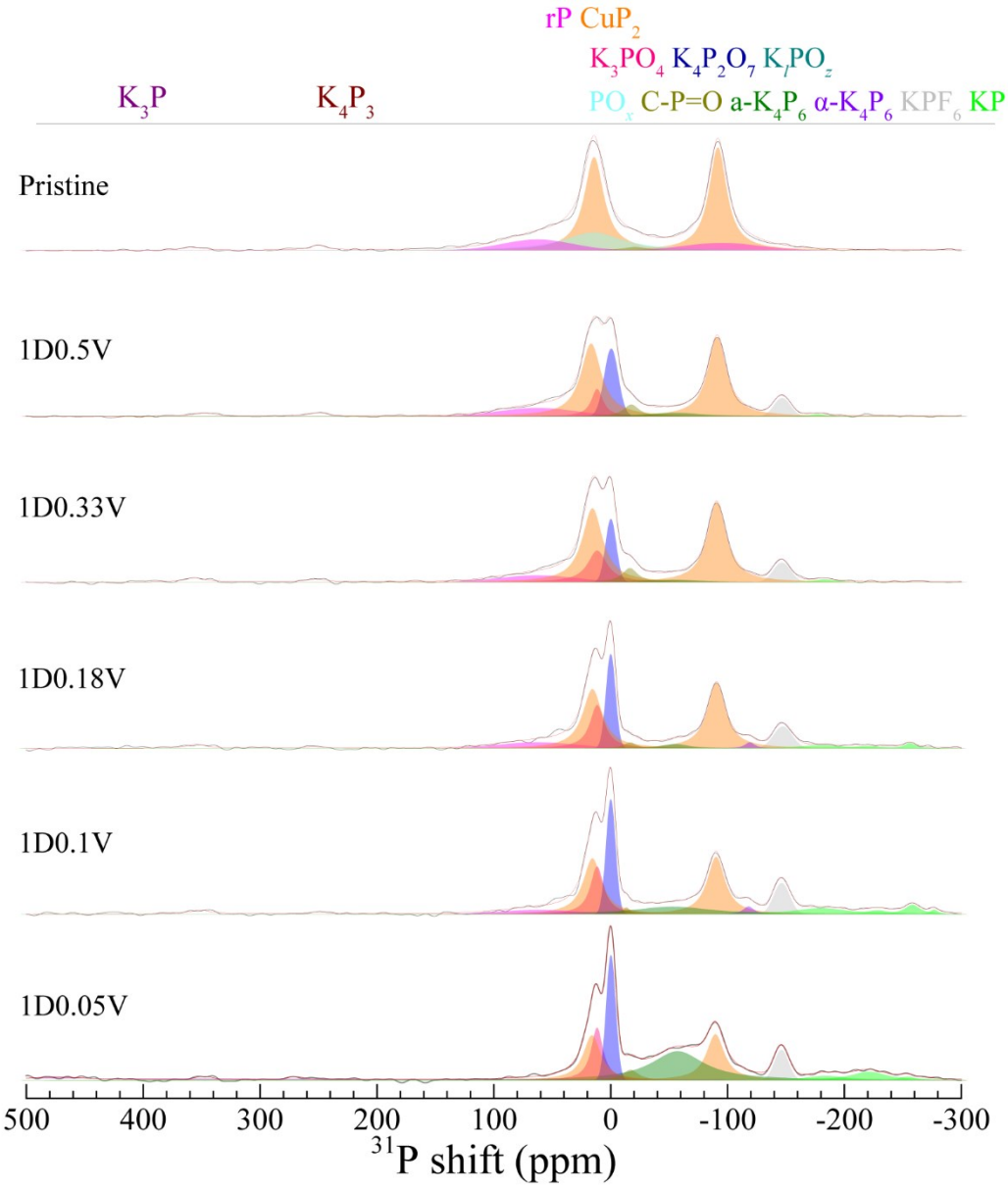

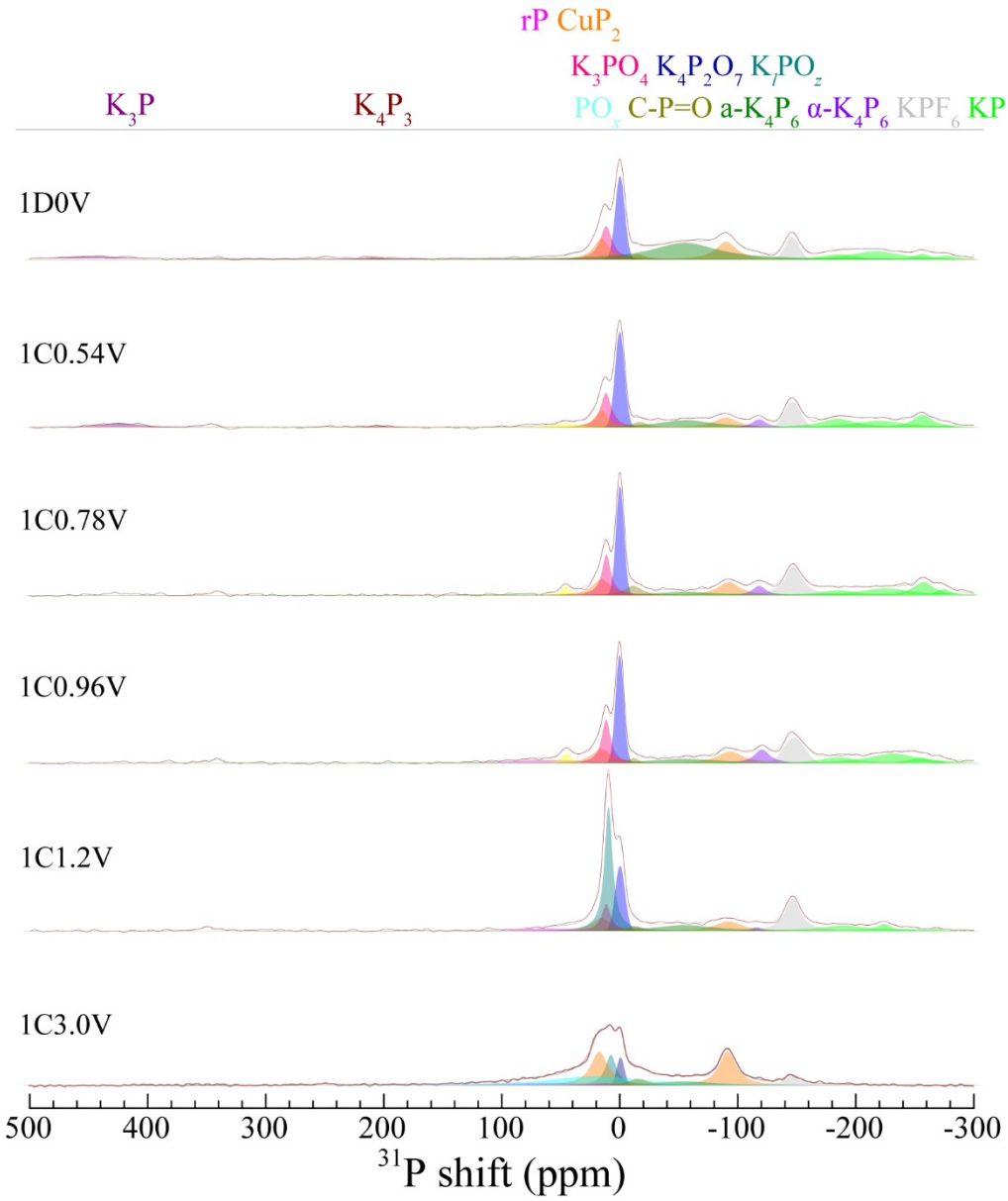
rP CuP2
K3PO4 K4P2O7 KlPOz
K3P
K4P3
POx C-P=O a-K4P6 α-K4P6 KPF6 KP
1D0V
1C0.54V
1C0.78V
1C0.96V
1C1.2V
1C3.0V
500
400
300
200
100
0
-100
-200
-300
31P shift (ppm)

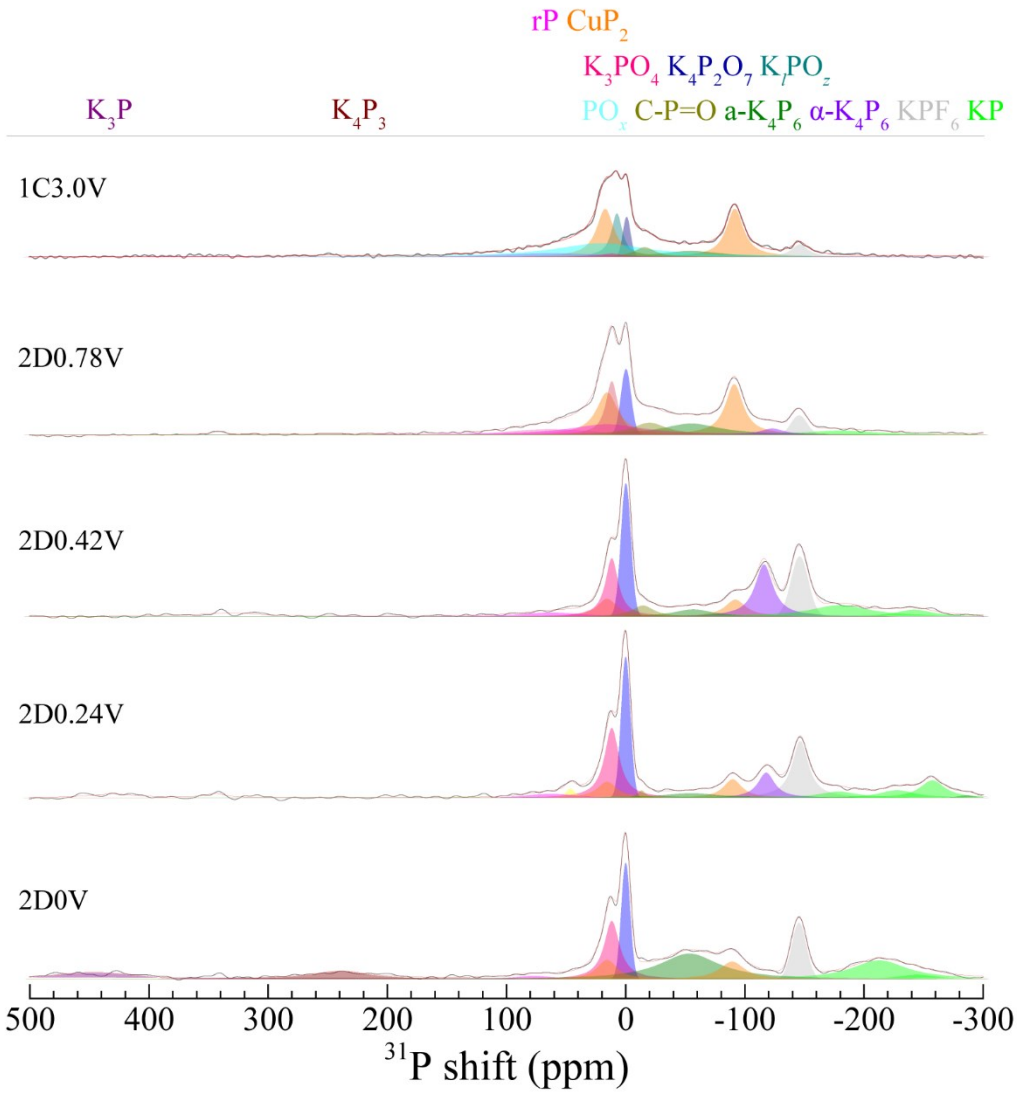
rP CuP2
K3PO4 K4P2O7 KxPOz
K3P K4P3 POx C-P=O a-K4P6 α-K4P6 KPF6 KP
1C3.0V
2D0.78V
2D0.42V
2D0.24V
2D0V
500 400 300 200 100 0 -100 -200 -300
31P shift (ppm)

References

1. Song, J.; Yu, Z.; Gordin, M. L.; Li, X.; Peng, H.; Wang, D., Advanced Sodium Ion Battery Anode Constructed via Chemical Bonding between Phosphorus, Carbon Nanotube, and Cross-Linked Polymer Binder. *ACS Nano* **2015,** *9* (12), 11933-11941.

2. Marino, C.; El Kazzi, M.; Berg, E. J.; He, M.; Villevieille, C., Interface and Safety Properties of Phosphorus-Based Negative Electrodes in Li-Ion Batteries. *Chem. Mater.* **2017,** *29* (17), 7151-7158.

3. Grimmer, A. R., ^{31}P NMR and π bond in solid phosphorus compounds. *Spectrochimica Acta Part A: Molecular Spectroscopy* **1978,** *34* (9), 941.

4. Hayashi, S.; Hayamizu, K., Spinning-rate dependence of ^{31}P magic-angle-spinning nuclear magnetic resonance spectra in condensed phosphates. *Chemical Physics* **1991,** *157* (3), 381-389.

5. Peng, C.; Chen, H.; Zhong, G.; Tang, W.; Xiang, Y.; Liu, X.; Yang, J.; Lu, C.; Yang, Y., Capacity fading induced by phase conversion hysteresis within alloying phosphorus anode. *Nano Energy* **2019,** *58*, 560-567.

6. Key, B.; Bhattacharyya, R.; Morcrette, M.; Sezne, V.; Tarascon, J.-M.; Grey, C. P., Real-Time NMR Investigations of Structural Changes in Silicon Electrodes for Lithium-Ion Batteries. *J. Am. Chem. Soc.* **2009,** *131*, 9239-9249.